

Monitoring a flooded open-cast mine with combining remote sensing techniques

Paulina Kujawa¹, Jaroslaw Wajs¹, Damian Kasza¹, Fabio Remondino²

¹ Department of Geodesy and Geoinformatics, Wrocław University of Science and Technology, Wrocław, Poland - (paulina.kujawa, jaroslaw.wajs, damian.kasza)@pwr.edu.pl

² 3D Optical Metrology (3DOM) unit, Bruno Kessler Foundation (FBK), Trento, Italy – remondino@fbk.eu

Keywords: Photogrammetry, LiDAR, Satellite imagery, Shoreline, Flooding, Open-cast mine.

Abstract

Monitoring environmental components at the land-water interface is very important for understanding as well as assessing dynamic hydrological and geomorphological processes. Such components include open-cast mines undergoing water reclamation. Three-dimensional modeling of these changing landscapes is essential to understand the dynamics of the water surface and to guide the safe reclamation process. Existing approaches often do not effectively integrate data from different platforms and sensors. This study presents a combined remote sensing technique that utilizes imagery and LiDAR-based data from UAVs, airborne, and satellite platforms to support the mapping of flooded mine. The proposed workflow involves data fusion, multi-temporal analysis, and 3D reconstruction to detect morphological changes, monitor hydrodynamic behaviour, and predict future flood scenarios. The results show that the combination of data from active and passive sensors significantly improves spatial and temporal resolution, enabling accurate and detailed modeling.

1. Introduction

Large environmental changes can affect the surrounding area of open-cast mines for many years after excavation/mining processes have ended. Some of these changes may have adverse consequences (e.g. land subsidence, soil erosion, or habitat loss), so it is essential to systematically monitor these areas. Monitoring the process of open-cast mine reclamation, especially in the case of water reclamation, allows geotechnical and hydrological risks to be assessed and predicted. In the literature, active and passive sensor technologies are commonly employed (Kubendiran and Ramaiah, 2024) for monitoring the flooded area. The choice of technology and sensors determines the types of analyses that can be performed as well as their accuracies. Depending on the type of collected data, analyses such as shoreline extraction, quantification of the flooded area (Nasser et al., 2024), morphological observation, and vegetation changes (Blachowski et al., 2023b) can be conducted. By using products such as Digital Terrain Models (DTMs) or Digital Surface Models (DSMs), in combination with GIS tools, it is possible to predict areas at risk of flooding (Osei et al., 2021).

1.1 Flooding dynamics

Monitoring the shoreline and tracking changes in water level is an effective way to control post-mining areas subjected to flooding. Point-wise height measurements can be taken using GNSS technology, and satellite or aerial imagery can be used for detailed analysis of water extent changes.

Methods for extracting water surface from RGB imagery include, among others edge-detection, machine learning, active contour model and polarization (Zhou et al., 2023). In a study by Vicens-Miquel et al. (2022), a method for automatically detecting wet/dry shorelines based on deep learning is proposed. In contrast, Garcia et al. (2023) developed a method for automatic segmentation of the extent of water using only RGB data within a simplified physical model.

Remote sensing indices are most commonly used in multispectral imaging to extract water surfaces. These indices are based on combinations of spectral bands, such as green, red, near-infrared (NIR), mid-infrared (MIR), and shortwave infrared (SWIR). Nasser et al. (2024) applied the Normalized Difference Water

Index (NDWI) and Normalized Difference Moisture Index (NDMI) to monitor the effects of flooding in post-mining areas. They classified the imagery into aquatic and terrestrial zones by applying an appropriate threshold. Similarly, Petropoulos et al. (2024) developed a threshold-based image processing technique using the NDWI and Modified Normalized Difference Water Index (MNDWI) to map flooded areas.

Although shoreline detection using LiDAR data is a common subject in scientific research, relatively few studies have focused on its application in flooded mining areas. Wang et al. (2023) outlined general shoreline extraction approaches, including methods based on proxy shoreline features, instantaneous shoreline detection, and multisource data fusion.

1.2 Morphological changes

Within open-cast mining excavations, after the closure of extraction, destructive processes (such as erosion and mass movements) as well as constructive ones (such as transport and sedimentation) often intensify. To assess these processes, researchers commonly use digital models derived from processed RGB imagery or LiDAR data. Padró et al. (2022) demonstrated the effectiveness of DEMs and orthophotos for identifying and quantifying erosion processes in reclaimed mining environments. In addition, this study examined slope maps to estimate erosion rates and determine their ranges. The analysis revealed a clear relationship between site topography and erosion intensity. Similarly, Blachowski et al. (2023a), employed UAV imagery and differential DEMs to analyse surface changes in gullies formed within a reclaimed lignite mine. The height models, created with a sub-centimetre precision, allowed for the quantification of material loss. In a study by Reinprech & Kieffer (2025), DSMs were used for morphometric feature extraction such as slope, curvature, roughness, dDEM (differential DEM), and dDSM (differential DSM) supporting the monitoring of mining areas and forested landslides zones.

1.3 Vegetation analyses

Multispectral imaging and vegetation indices are commonly used for monitoring vegetation dynamics in the reclaimed area. These indices support the assessment of ongoing reclamation, detection of vegetation anomalies and evaluation of the impact of mining

activities on vegetation cover. Multispectral data from various sensors can be compared and correlated to provide detailed information through long-term monitoring. In the study by Hu et al. (2022), data from Landsat 8, Sentinel-2, and HJ1A sensors were used to compare vegetation indices in a reclaimed mining area. Similarly, Buczyńska et al. (2023), analysed vegetation conditions in a post-mining landscape and modeled the relationship between historical mining activities and vegetation changes. The authors used several vegetation indices, including the Normalized Difference Vegetation Index (NDVI), Normalized Difference Infrared Index (NDII), and the Modified Triangular Vegetation Index – Improved (MTVI2). Also, Reinprech & Kieffer (2025) used multispectral UAV imagery to identify differences in vegetation density and growth rates in former mining areas by determining indices such as NDVI and NDWI.

1.4 Predictions

Forecasting future processes on reclaimed mine sites is crucial, especially in the context of water reclamation, where ensuring safety is particularly important. UAV data and GIS tools can successfully assess geohazard risk. For instance, Mao et al. (2024) performed a quantitative landslide risk analysis in loess areas, considering drivers and triggers such as roads, rivers, groundwater, slope, and lithology. They assessed landslide risk for different precipitation scenarios and return times. In contrast, Qing et al. (2025) presented a novel approach to landslide prediction in open-cast mines, integrating UAV data, GIS tools, 3D geological modeling, machine learning, and numerical simulations to provide a detailed and interpretable assessment of slope hazards.

1.5 Paper's aim

The aim of this study is to integrate remote sensing data for comprehensive monitoring of a flooding process in a reclaimed open-cast mine. Based on both collected and open-source data, key analyses and observations include:

- (i) hydrodynamic changes, e.g. delineating shorelines, calculating reservoir area and estimating volume changes based on RGB images, LiDAR data and multispectral data from Sentinel-2;
- (ii) morphological changes based on RGB images and LiDAR data;
- (iii) land cover detection based on multispectral imagery;
- (iv) prediction of further water rise as well as identification of high-risk zones of significant morphological changes.

The entire methodology is shown in Figure 1 and reported in Section 3.

2. Study area and datasets

The paper related to the implementation of a periodic monitoring project at the Stanisław Mine (SW Poland), specifically focusing on the Stanisław-South excavation site. This post-mining excavation is undergoing water reclamation. The primary source of water inflow into the excavation site is precipitation, with groundwater inflows playing a secondary role. Due to the properties of the clay soils, which form an impermeable isolating layer, visible erosion features caused by surface runoff and concentrated groundwater inflows can be observed in the basin of the filling excavation, particularly in its southern part. Water reclamation has been ongoing since 2023.

The data used for the geodetic monitoring are presented in Table 1. For in situ UAV measurements, two types of platforms/sensors were used: (i) a DJI Phantom 4, equipped with a 20-megapixel

digital camera, and (ii) a DJI Matrice 300, equipped with a miniVUX-3 UAV laser scanner.

Technology	Date of measur.	Type of data	GSD / Resolution
ALS	02.04.2019	LiDAR	8 pts/m ²
UAV	02.12.2022	RGB images	0.05 m
	13.09.2023	RGB images	0.05 m
	21.10.2024	LiDAR + RGB images	120 pts/m ²
Satellite	01.04.2019	S2 imagery (13 bands)	10
	06.11.2022	S2 imagery (13 bands)	10
	12.09.2023	S2 imagery (13 bands)	10
	26.10.2024	S2 imagery (13 bands)	10

Table 1. Description of the used datasets.

3. Methods

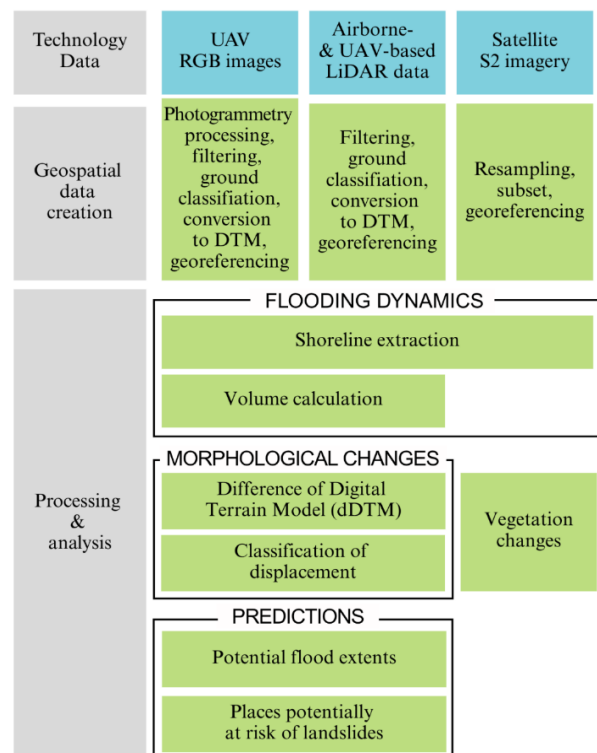


Figure 1. Workflow of the proposed methodology.

3.1 Geospatial data collection and creation

The first stage of the proposed methodology involves few processing steps to generate geospatial data for subsequent analysis. UAV images were processed using a standard photogrammetric pipeline supported by GCPs for scaling and georeferencing purposes.

LiDAR data from the UAV were filtered manually to eliminate noise in the water surface area caused by single plants and sticks and registered water surface points. RGB images were used to colorize the LiDAR point cloud from UAV. As no GCPs were available, the alignment of the images relied solely on the data from the camera positions. The image-based point cloud was then aligned to the LiDAR dataset using an Iterative Closest Point (ICP) algorithm. RGB values were then transferred to the LiDAR points via spatial, proximity-based interpolation. Airborne LiDAR data over the AOI were extracted from the national geoportal (www.geoportal.gov.pl).

To generate DTMs, ground points from LiDAR and photogrammetric processing were extracted during the classification process. The resolution of each DTM was defined based on the density of the point cloud, ensuring terrain detail was preserved while avoiding unnecessary data redundancy. In some cases, the terrain models were aggregated to ensure compatibility with specific types of analysis - for instance, when comparing datasets from different time periods or performing correlation analyses.

Sentinel-2 L2A images were downloaded from the Copernicus Data Space Ecosystem Browser. They were resampled and reprojected. The final step for all data was the transformation into a common coordinate system.

3.2 Flooding dynamics

Flood dynamics were assessed based on shoreline changes derived from the 3D model. A manual segmentation process was applied to the RGB images obtained from the UAV. Coarse shoreline points were identified on the point cloud and verified using the orthomosaics. A plane representing the water surface was then fitted to these extracted points and dense shoreline points were extracted using the C2M comparison. Due to the dense vegetation along the shoreline, polygons representing the water surface were manually drawn. For both UAV and ALS LiDAR data, the water extent extraction process was performed similarly. In the case of airborne LiDAR, water points identified during the classification process were used as coarse shoreline points. A plane was then fitted to these points, and the subsequent steps followed the same procedure as for UAV imagery. For Sentinel-2 imagery, the NDWI index (Eq. 1) was used to extract the water area.

$$NDWI = \frac{GREEN - NIR}{GREEN + NIR} \quad (1)$$

Next, the raster representing the water area was converted into polygon and smoothed to eliminate sharp angles. The water surface area was calculated based on the generated polygons.

The increase in water volume for each period was also calculated. To determine this, two surface models were compared: a reference model representing the baseline area and a water surface model corresponding to the flood extent of the target period. By calculating the enclosed volume between the two surfaces, the change in water volume over time was established.

3.3 Morphological changes

Changes in ground elevation were analysed using the differential DTM (dDTM) approach. This method involves subtracting DTMs generated during different measurement epochs to quantify vertical changes in surface elevation, as well as detect and assess subsidence or uplift processes. To better interpret the intensity of terrain changes in the study area, a classification scheme was applied to the dDTM results. The terrain was divided into six classes based on morphological change. These classes distinguish between significant, very significant, and extreme changes in terrain. The classification criteria and corresponding elevation change ranges are provided in Table 2.

Class	Value
Extreme subsidence	< - 2 m
Very significant subsidence	-2 to -1 m
Significant subsidence	-1 to 0 m
Significant uplift	0 to 1 m

Very significant uplift	1 to 2 m
Extreme uplift	> 2 m

Table 2. Classification of morphological changes based on vertical elevation differences.

3.4 Vegetation changes

In addition, vegetation dynamics were analysed by calculating the NDVI index (Eq. 2) from Sentinel-2 imagery.

$$NDVI = \frac{NIR - RED}{NIR + RED} \quad (2)$$

As shown in Table 3, five land cover classes were distinguished based on NDVI index thresholds adapted from Vorovencia (2021). To improve the accuracy of delineating the water surface, especially in areas with ambiguous reflectance values, the NDWI was also used. The water mask derived from the NDWI was integrated with the NDVI-based classification through a mosaic operation. This combination minimized the misclassification of water surfaces in vegetated regions, improving the classification results' overall reliability.

Class	Value
No vegetation / water	< 0.0
Barren land	0.0 – 0.1
Sparse grass	0.1 – 0.2
Grass and shrubs	0.2 – 0.3
Mixed vegetation	< 1

Table 3. NDVI classes.

3.5 Predictions

The initial stage of the predictive analysis involved determining the potential extent of flooding at different water levels. Based on the latest DTM from 2024, the spatial extent of flooding was estimated for progressive increases in water level (by 1 m, 2 m, 5 m and 10 m) and the corresponding water volume was calculated. This information is particularly valuable in the context of managed reclamation, as it enables the precise estimation of the volume of water (in cubic metres) required to inundate the post-mining area to a certain height.

In the second prediction processing, the dDTM and slope data were used to identify areas prone to surface deformation. For each dDTM layer, zones of significant uplift (>1 m) and subsidence (< -1 m) were extracted and then combined to highlight areas that experienced significant changes in elevation over time. In the following step - these deformation zones were compared with areas where the slope exceeded 20 degrees, as well as regions of barren land and sparse grass identified from satellite imagery. The resulting overlaps represent potential risk zones.

4. Results

4.1 Geospatial data

The photogrammetric processing of the collected UAV images (Table 4) produced dense point clouds, elevation models and orthomosaics. Errors in object space (RMSE) are in the order of the image GSD for the 2022 datasets due to a non-optimal imaging geometry. After ground point classification, the number of points in the cloud was reduced, and the spatial resolution was recalculated. The aggregated resolution, along with the adjusted resolutions used for subsequent analyses, is presented in Table 5.

Date	2022	2023
Number of images	429	761
Image resolution [pix]	5472 x 3648	5472 x 3648
Image GSD [cm/pix]	3.1	2.6
RMSE [cm] / [pix]	3.4 / 1.1	1.2 / 0.4

Table 4. UAV image acquisitions and bundle adjustment results for the 2022 and 2023 campaigns.

Type on analysis	Data / model used	Date	Resolution / density
Shoreline extraction	Point clouds (pre-classification)	2019, 2022, 2023, 2024	8, 305, 370, 120 pts/m ²
	S2 imagery	2019, 2022, 2023, 2024	10 m
Volume	DTM	2019, 2022, 2023, 2024	80, 15, 15, 30 cm
Morphological changes	dDTM; DTM slope vs. dDTM	2019-2022, 2022-2023, 2023-2024	80, 15, 30 cm
Vegetation changes	NDVI / NDWI rasters	2019, 2022, 2023, 2024	10 m
	Vegetation cover vs. dDTM	2019-2022, 2022-2023, 2023-2024	10 m
Predictions	Water surface cover (DTM)	2024	30 cm
	High-risk zone detection (DTM)	2024	80 cm

Table 5. DSM resolutions adopted for the respective analyses.

4.2 Flooding dynamics

The interpolated shorelines (Figure 2) clearly show a progressive increase in water surface area over the analysed period. The largest increase was observed between 2019 and 2022, when the reservoir was intensively filled, reaching a volume of approximately 448,879 m³. In 2023, the area of the reservoir increased by 9,302 m², while in 2024 it increased by a further 3 ha, which resulted in an increase in water volume of about 246,425 m³. Detailed quantitative data is provided in Table 6.

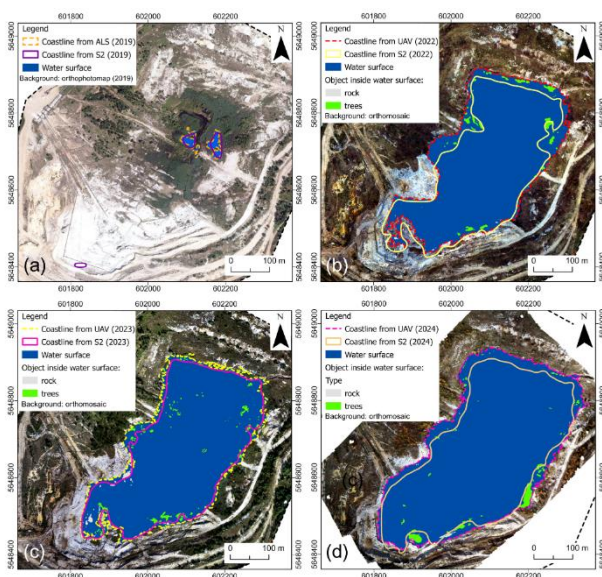


Figure 2. Reservoir shorelines generated based on UAV, ALS and satellite data: (a) 2019, (b) 2022, (c) 2023, and (d) 2024.

Date	Sensor	Water area [m ²]	Increase volume [m ³]
2019	ALS S2	2332 2186	-
2022	UAV S2	116478 102013	+469636
2023	UAV S2	125780 114025	+99248
2024	UAV S2	155862 132097	+244561 -

Table 6. Statistics presenting the dynamics of changes in a flooded open-cast mine.

A comparison of water areas extracted from Sentinel-2 satellite data and UAV imagery revealed an average difference of 12%. The high correlation coefficient ($r = 0.968$) confirmed the strong agreement between the two data sets. However, the greatest discrepancies in shoreline position were observed in vegetated areas. This is mainly due to the lower resolution of the satellite imagery, which leads to generalization of the results. Additionally, emergent vegetation above the water surface but not in direct contact with land was classified as land area in the analysis using the NDWI index. In such cases, the boundary between water and vegetation was too narrow for processing based on spectral values to detect it correctly.

4.3 Morphological changes

Comparison of the dDTM models (Figure 3) not only allowed changes to be observed but also helped to identify areas with significant erosion and sedimentation processes. In the 2019-2022 period, the water level rose by more than 4 metres, and landslides in the south-western part of the AOI are particularly evident. In some locations, displacements of up to 8 meters were reported.

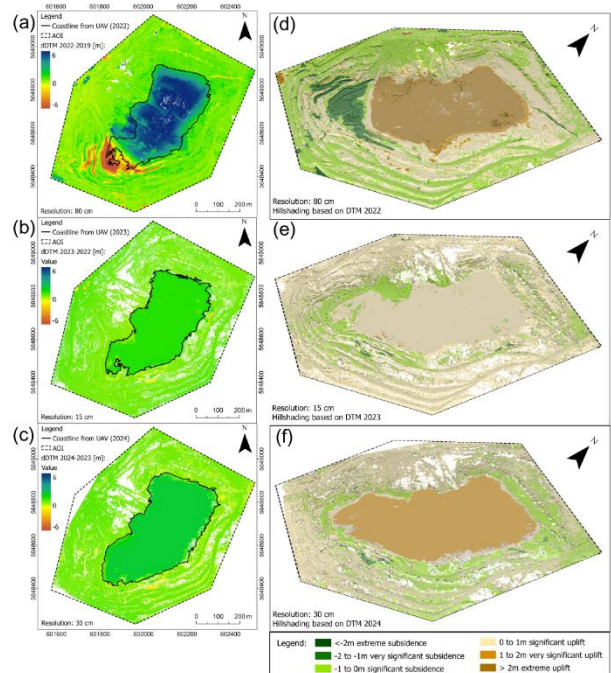


Figure 3. dDTM (a-c) and classification of displacement based on significance (d-f) for: (a, d) 2019–2022, (b, e) 2022–2023, and (c, f) 2023–2024.

During the next period, from 2022 to 2023, the water level increased by about 0.8 meters. This was accompanied by significant additional mass movements around the reservoir. Small landslides with an amplitude of displacement of approx. 2 meters were identified in the southern and southeastern part of the AOI. Additionally, a new zone of deformation emerged in the eastern region of the reservoir, with maximum displacements reaching 4 meters.

In the final analysed time interval, from 2023 to 2024, the water level increased sharply by 1.8 meters. Zones of landslide activity remained largely coincident with those previously identified, reaching similar displacement values.

An analysis was conducted to investigate the relationship between land displacement (dDTM) and slope (Figure 4). To avoid misinterpreting uplift caused by hydraulic reclamation, areas subjected to water reclamation were excluded. From 2019 to 2022, significant subsidence and uplift mainly occurred on gentle slopes (mean: 11.76° and 12.49°, respectively), with extreme changes near 10°, which indicates large-scale land movement. Between 2022 and 2023, significant uplift and subsidence began to dominate on slightly steeper slopes (approximately 14°), probably reflecting the ongoing reshaping and subsidence of the fill. These changes continued between 2023 and 2024. The overall trend suggests increasing surface stability and ongoing reclamation success.

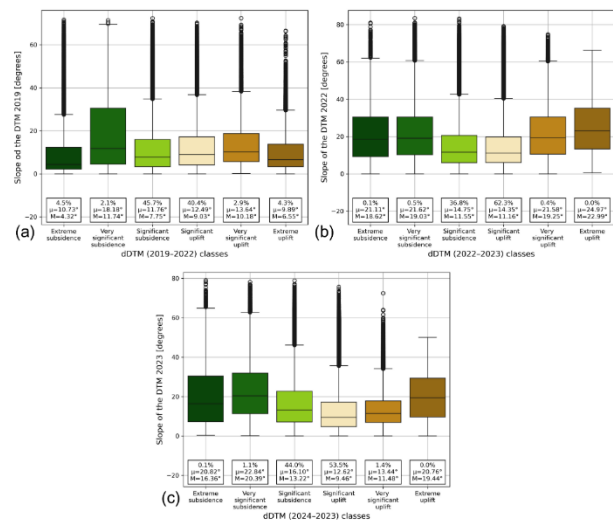


Figure 4. Relationship between slope of the DTM and dDTM: (a) 2019-2022, (b) 2022-2023, (c) 2023-2024.

4.4 Vegetation changes

As shown in Figure 5, clay extraction was still being carried out in 2019, as evidenced by the presence of barren land (18.5%) and sparse grass (38.6%). In subsequent years, the flooded area expanded, reaching 19.2% in 2022. This expansion had a dual effect on the local landscape. First, some vegetated zones were submerged, including areas of grass and shrubs. Second, it stimulated the growth of mixed vegetation around the reservoir, which reached 53.1% in 2022. Although mixed vegetation decreased in 2023, it recovered in 2024. Sparse grass and barren land consistently declined over time.

Analyzing the change in vegetation between 2019 and 2024 clearly illustrates the effects of water reclamation. There has been a transition from predominantly terrestrial environment to aquatic and mixed-vegetation ecosystems, which enhances habitat diversity in the reclaimed landscape.

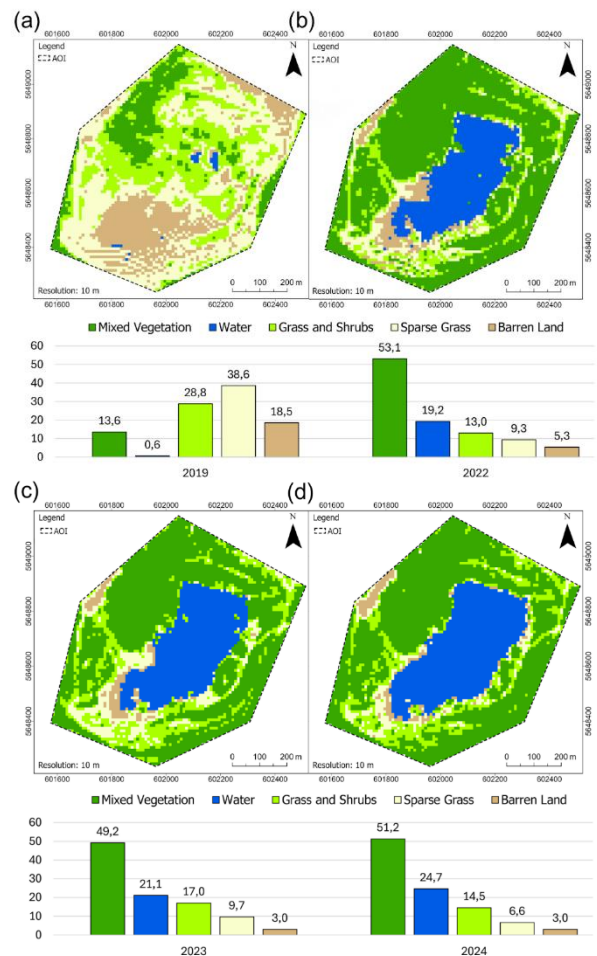


Figure 5. Vegetation cover based on NDVI and NDWI in (a) 2019, (b) 2022, (c) 2023, and (d) 2024.

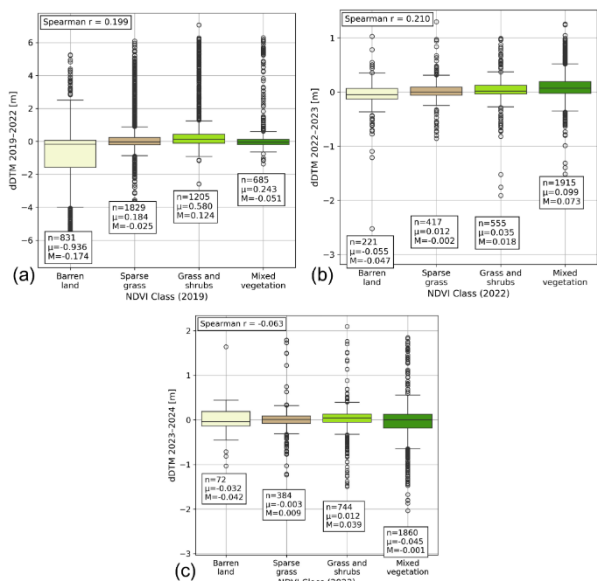


Figure 6. Relationship between vegetation cover and dDTM: (a) 2019-2022, (b) 2022-2023, (c) 2023-2024.

A correlation analysis was carried out between the observed displacement values for each year and the NDVI values before deformation (Figure 6). For this reason, all datasets were aggregated to a spatial resolution of 10 metres. For the period from 2019 to 2022, a weak yet significant trend emerged. It

indicates that increased vegetation leads to reduced erosion and greater stability. This theory is also supported by degraded barren land, where the average displacement value was -0.936 m. Analysis of the 2022-2023 period revealed a weak but statistically significant trend. Once again, erosion was lower in areas with mixed vegetation. There is no clear trend in the final analysed period, which may be related to the stabilization of the area and the healthy vegetation dominating the reclaimed study area.

4.5 Predictions

Further increase in water level is expected in the study area as a result of ongoing water reclamation. It is crucial to monitor the site and mitigate the negative effects of rapid landform changes. To achieve this, the potential extent of water should be observed (Figure 7). Based on the current water surface area of $155,862$ m² (from 2024) and the total volume increase of $813,445$ m³ (from 2019), further simulations indicate that increasing the water level by 1 meter would expand the surface area to $166,893$ m² and add approximately $160,123$ m³ of water. Conversely, a potential 10-meter increase would result in an area of $241,199$ m² and a cumulative volume increase of over 2 million m³.

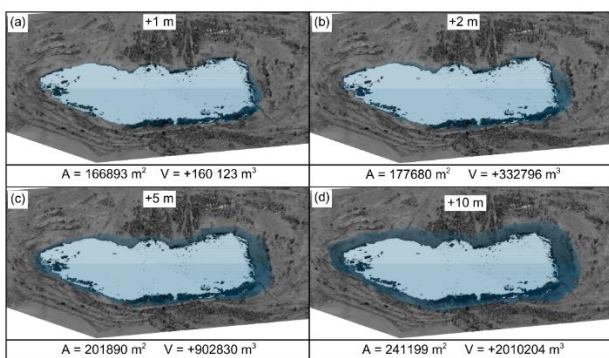


Figure 7. Prediction of water surface cover on the 2024 DSM model after an increase of (a) 1 m, (b) 2 m, (c) 5 m, and (d) 10 m.

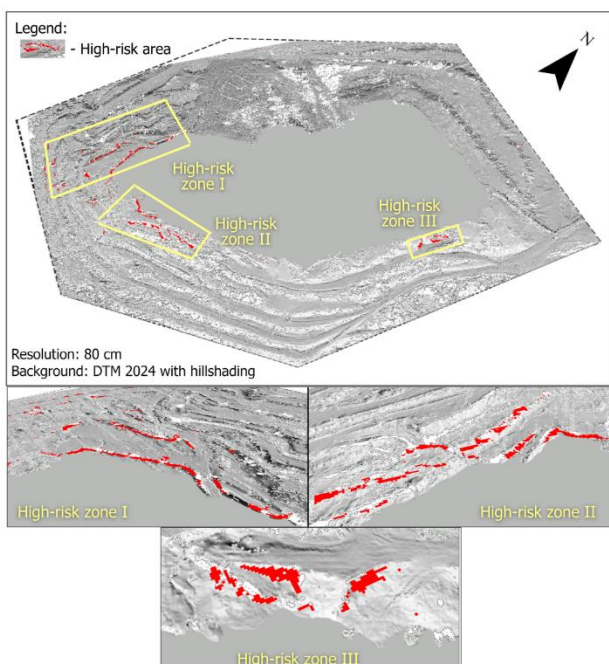


Figure 8. High-risk zone detection based on DTM from 2024 analysis.

It is also necessary to analyse the terrain and its slope. Figure 8 shows the potential locations of significant subsidence. Three key high-risk zones were identified. These zones are located near the reservoir, making it especially important to monitor them in the event of further flooding.

5. Discussion and conclusions

Remote sensing data are widely used to monitor mining areas, especially those undergoing reclamation and characterised by dynamic environmental changes. Flooded areas require special attention, and the fusion of data from different sources - UAV, airborne, and satellite - provides a comprehensive observation that allows for ongoing monitoring and evaluation of restoration efforts, as well as a rapid response to any concerning changes.

The approach proposed in this study is an important contribution to the field of post-mining land reclamation. It introduces a comprehensive, repeatable workflow for monitoring and assessing reclamation progress, particularly with regard to water reclamation. Integrating data from various sources — UAV, LiDAR, and Sentinel-2 — enables precise tracking of shoreline dynamics, estimation of water volume changes in flooded areas, assessment of morphological land transformations (including displacements), analysis of vegetation cover dynamics and state, and forecasting of future geomorphological and hydrological processes. In the long term, the proposed methodology can support decision-making in the planning and execution of reclamation activities, particularly those related to water management. It can also provide a basis for reclamation policies that aim to restore and maintain sustainable environmental conditions.

High-resolution UAV images and LiDAR data were essential in this research to provide the best possible accuracy and resolution. However, the proposed methodology is not limited to UAV-based data only. It can be adapted to use aerial images or existing elevation models available from national portals or other spatial data providers. This flexibility enables the workflow to be used in various scenarios, depending on the available instruments, data and the scale of the study area.

It is possible to accurately extract the water surface from processed RGB images acquired by a UAV using a simple manual workflow with GIS tools. This method is particularly relevant when direct shoreline measurements using GNSS techniques are impossible or extremely difficult. Although satellite multispectral images are an excellent alternative to photogrammetry, their accuracy is, on average, about 12% lower due to their lower spatial resolution. An additional limitation is the need for cloud-free imagery. Additionally, shoreline classification may be inaccurate due to the presence of submerged vegetation. Although such vegetation does not form the actual shoreline, it can be misclassified as land area, especially if it is located near the shore.

The 3D models obtained from photogrammetric and LiDAR processing allow the assessment of morphological changes taking place around the reservoir. The accuracy of the dDTM method primarily depends on the georeferencing, spatial resolution, and precision of the data used to create digital models. The dDTM approach achieves very high accuracy using high-resolution data, such as models generated from UAV photogrammetry or LiDAR scanning. The analyses presented here are based on data with a spatial resolution in the range of 10-60 cm. This resolution enables the detection of significant

morphological changes, including surface erosion, sedimentation, and ground subsidence. Several key advantages of this method over other techniques should be highlighted: greater spatial coverage than point-based GNSS data collection, higher spatial resolution than radar techniques such as InSAR, and more efficient and non-invasive data collection than terrestrial laser scanning. In summary, using high-quality digital models in combination with dDTM differential analysis provides an effective, accurate tool for monitoring land dynamics at local and medium scales.

Multispectral imaging, which allows analysis of vegetation changes, is of added value in monitoring post-mining areas. The analysed reclaimed mine area shows an increase in aquatic areas and mixed vegetation. This indicates positive natural ecological succession. The disappearance of barren soil and sparse grass and the development of mixed vegetation around the reservoir suggest improved habitat conditions and the formation of new ecosystems. Mixed vegetation may promote slope stabilization and reduce erosion. However, the high-risk zone prediction analysis shows that there are still areas where deformation may occur. These areas should be monitored in the future.

The methods proposed in this study can be successfully applied to other mining areas with different environmental conditions and problems. The developed workflow combines UAV, LiDAR, and Sentinel-2 data with commonly available, user-friendly GIS tools, allowing it to adapt to different landscapes. Its modular, repeatable structure enables users to customize their input data, classification schemes, and spatial resolutions according to their sensors and the unique characteristics of their study area. This flexibility makes the methodology suitable for a wide range of post-mining environments undergoing various reclamation processes.

Future studies of the Stanislaw Mine site will include bathymetric measurements using an echo sounder. This data will enable us to assess the dynamics of morphological changes to the bottom over time, identify accumulation and erosion zones, and improve our understanding of the processes that occur during and after water reclamation.

6. References

- Blachowski, J., Becker, M., Kujawa, P., Koźma, J., Warchala, E., Dynowski, A., Pawlik, M., Wajs, J., & Buczyńska, A., 2023a. Transformation processes in lignite post-mining landscape - erosion of anthropogenic formations in the former “Przyjazn Narodow – Szyb Babina” mine (Poland). *Zeitschrift Der Deutschen Gesellschaft Für Geowissenschaften*, 173(4), 565–580.
- Blachowski, J., Dynowski, A., Buczyńska, A., Ellefmo, S. L., & Walerysiak, N., 2023b. Integrated Spatiotemporal Analysis of Vegetation Condition in a Complex Post-Mining Area: Lignite Mine Case Study. *Remote Sensing*, 15(12), 3067.
- Buczyńska, A., Blachowski, J., & Bugajska-Jędraszek, N., 2023. Analysis of Post-Mining Vegetation Development Using Remote Sensing and Spatial Regression Approach: A Case Study of Former Babina Mine (Western Poland). *Remote Sensing*, 15(3), 719.
- García, M., Alcayaga, H., & Pizarro, A., 2023. Automatic Segmentation of Water Bodies Using RGB Data: A Physically Based Approach. *Remote Sensing*, 15(5), 1170.
- Hu, J., Ye, B., Bai, Z., & Hui, J., 2022. Comparison of the Vegetation Index of Reclamation Mining Areas Calculated by Multi-Source Remote Sensing Data. *Land*, 11(3), 325.
- Kubendiran, I., & Ramaiah, M., 2024. Modeling, Mapping and Analysis of Floods Using Optical, Lidar and SAR Datasets—a Review. *Water Resources* 51(4), 438–448.
- Mao, Z., Yu, H., Ma, X., Liang, W., Gao, G., Tian, Y., & Shi, S., 2024. Refinement analysis of landslide risk assessment for wide area based on UAV-acquired high spatial resolution images. *Stochastic Environmental Research and Risk Assessment*.
- Nasser, F. de C., Mello, D. C. de, Francelino, M. R., Krause, M. B., Soares, H. de M., & Demattê, J. A. M., 2024. Mapping deactivated mine areas in the amazon forest impacted by seasonal flooding: Assessing soil-hydrological processes and quality dynamics by remote sensing and geophysical techniques. *Remote Sensing Applications: Society and Environment*, 34, 101148.
- Osei, B. K., Ahenkorah, I., Ewusi, A., & Fiadonu, E. B., 2021. Assessment of flood prone zones in the Tarkwa mining area of Ghana using a GIS-based approach. *Environmental Challenges*, 3, 100028.
- Padró, J.-C., Cardozo, J., Montero, P., Ruiz-Carulla, R., Alcañiz, J. M., Serra, D., & Carabassa, V., 2022. Drone-Based Identification of Erosive Processes in Open-Pit Mining Restored Areas. *Land*, 11(2), 212.
- Petropoulos, G. P., Georgiadi, A., & Kalogeropoulos, K., 2024. Leveraging Sentinel-2 and Geographical Information Systems in Mapping Flooded Regions around the Sesia River, Piedmont, Italy. *GeoHazards*, 5(2), 485–503.
- Qing, L., Xu, L., Huang, J., Fu, X., & Chen, J., 2025. Intelligent Prediction and Numerical Simulation of Landslide Prediction in Open-Pit Mines Based on Multi-Source Data Fusion and Machine Learning. *Sensors*, 25(10), 3131.
- Reinprecht, V., & Kieffer, D. S., 2025. Application of UAV Photogrammetry and Multispectral Image Analysis for Identifying Land Use and Vegetation Cover Succession in Former Mining Areas. *Remote Sensing*, 17(3), 405.
- Vorovencii, I., 2021. Changes detected in the extent of surface mining and reclamation using multitemporal Landsat imagery: a case study of Jiu Valley, Romania. *Environmental Monitoring and Assessment*, 193(1).
- Wang, J., Wang, L., Feng, S., Peng, B., Huang, L., Fatholahi, S. N., Tang, L., & Li, J., 2023. An Overview of Shoreline Mapping by Using Airborne LiDAR. *Remote Sensing*, 15(1), 253.
- Zhou, X., Wang, J., Zheng, F., Wang, H., & Yang, H., 2023. An Overview of Coastline Extraction from Remote Sensing Data. *Remote Sensing*, 15(19), 4865.